Author Manuscript

Author Manuscript

Author Manuscript

Author Manuscript

HHS Public Access

Author manuscript

Cell Stem Cell. Author manuscript; available in PMC 2016 November 05.

Published in final edited form as:

Cell Stem Cell. 2015 November 5; 17(5): 569–584. doi:10.1016/j.stem.2015.08.003.

Genome-Wide RNA-Seq of Human Motor Neurons Implicates Selective ER Stress Activation in Spinal Muscular Atrophy

Shi-Yan Ng[1,2,5], **Boon Seng Soh**[1,2,3,5], **Natalia Rodriguez-Muela**[1,2], **David G. Hendrickson**[1,4], **Feodor Price**[1,2], **John L. Rinn**[1,4], and **Lee L. Rubin**[1,2,#]

[1]Department of Stem Cell and Regenerative Biology, Harvard University, Cambridge, MA 02138

[2]Harvard Stem Cell Institute, Cambridge, MA 02138

[3]Department of Cell and Molecular Biology, Karolinska Institute, Stockholm, Sweden SE-17177

[4]The Broad Institute of Massachusetts Institute of Technology and Harvard, Cambridge, MA 02142

SUMMARY

Spinal Muscular Atrophy (SMA) is caused by mutations in the *SMN1* gene. Because this gene is ubiquitously expressed, it remains poorly understood why motor neurons (MNs) are one of the most affected cell types. To address this question, we carried out RNA-sequencing studies using fixed, antibody-labeled and purified MNs produced from control and SMA patient-derived induced pluripotent stem cells (iPSCs). We found SMA-specific changes in MNs, including hyper-activation of the endoplasmic reticulum (ER) stress pathway. Functional studies demonstrated that inhibition of ER stress improves MN survival *in vitro* even in MNs expressing low SMN. In SMA mice, systemic delivery of an ER stress inhibitor that crosses the blood-brain-barrier led to preservation of spinal cord MNs. Therefore, our study implies that selective activation of ER stress underlies MN death in SMA. Moreover, the approach we have taken would be broadly applicable for studying disease-prone human cells in heterogeneous cultures.

Graphical Abstract

[#]Corresponding author: Lee L. Rubin, lee_rubin@harvard.edu.

[5]These authors contributed equally to the work

AUTHOR CONTRIBUTIONS

SYN, BSS, JLR and LLR designed the study; SYN, BSS, NRM, DGH and FDP carried out the experiments and analyzed data. SYN and LLR wrote the manuscript, and all authors read the paper.

Publisher's Disclaimer: This is a PDF file of an unedited manuscript that has been accepted for publication. As a service to our customers we are providing this early version of the manuscript. The manuscript will undergo copyediting, typesetting, and review of the resulting proof before it is published in its final citable form. Please note that during the production process errors may be discovered which could affect the content, and all legal disclaimers that apply to the journal pertain.

Author Manuscript Author Manuscript Author Manuscript Author Manuscript

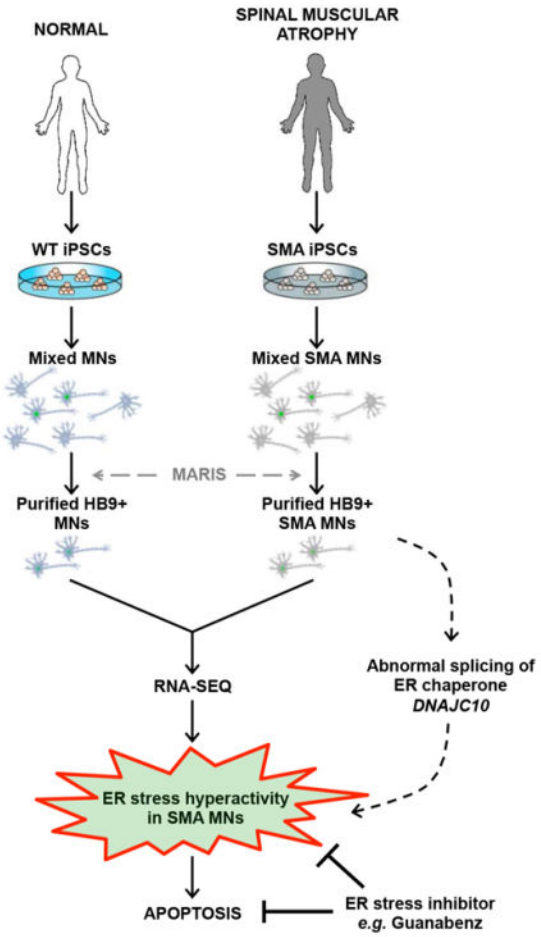

INTRODUCTION

Spinal muscular atrophy (SMA) is a genetic motor neuron (MN) degenerative disease and is the leading genetic cause of infant mortality. SMA is caused by mutations in the *SMN1* gene, resulting in reduced levels of Survival Motor Neuron (SMN) protein. This causes the selective loss of spinal cord MNs and denervation of skeletal muscles, eventually leading to muscular atrophy and death. Humans contain two *SMN* genes (*SMN1* and *SMN2*), with the duplicated *SMN2* gene behaving as a disease modifier because it predominantly gives rise to an exon 7-skipped mRNA that produces a truncated SMNΔ7 protein, together with a small fraction of the full-length, functional SMN protein (Burghes and Beattie, 2009). The severity of the disease is inversely correlated with SMN protein levels, and it has been well established that loss of SMN function recapitulates the disease while restoring full-length SMN protein reverses the SMA phenotype (Corti et al., 2012; Ebert et al., 2009; Foust et al., 2010). However, it remains unclear why the loss of SMN, a ubiquitously-expressed protein, results in the selective death of motor neurons (MNs). This raises the possibility that MNs possess unique properties that render them more sensitive to low levels of SMN. The question of cell type selectivity underlies many neurodegenerative diseases, and the use of

Author Manuscript Author Manuscript Author Manuscript Author Manuscript

induced pluripotent stem cells (iPSCs) now makes it possible to begin to understand how this is achieved. Disease relevant cell types can be derived from patients and control subjects by directed differentiation of these iPSCs, providing an *in vitro* platform for discovery of disease-associated phenotypes. However, these studies are often complicated by the fact that neuronal cultures tend to be quite heterogeneous. For example, MN cultures are "contaminated" by the presence of other types of spinal cord neurons and glial cells. In some sense this is advantageous because it preserves a more *in vivo*-like environment. Nonetheless, the presence of other cells complicates the identification of specific changes that might occur preferentially in the MNs for which there are no known cell-surface markers to allow their purification by flow cytometry.

In order to address the MN-specific degeneration in SMA, we used a method to purify MNs based on intracellular protein labeling (Hrvatin et al., 2014). Through RNA-sequencing of purified MNs, we identified gene expression changes in normal versus SMA MNs. Gene clustering revealed that SMA MNs express high levels of apoptotic genes as well as genes involved in the endoplasmic reticulum (ER) stress pathway. We also found that loss of SMN specifically activates the unfolded protein response (UPR) in the MN population, which may be somewhat surprising since SMA is one of the few neurodegenerative diseases not characterized by protein misprocessing and aggregate formation. It appears that MNs are chronically more susceptible to ER stress (Kiskinis et al., 2014), and the loss of SMN exacerbates this condition further. Notably, small molecule antagonists of the ER stress pathway promote SMA MN survival both *in vitro* and *in vivo*, and partially rescues the SMA phenotype without changing SMN levels. Our data indicate that the UPR is selectively activated in SMN-deficient MNs, eventually leading to motor neuron death. This study also serves as a proof-of-principle that intracellular-based sorting strategies can be applied to understand the pathogenesis of human diseases affecting selective cell types.

RESULTS

MNs generated from SMA patient iPSCs show a pro-apoptotic phenotype

We generated iPSCs from primary fibroblasts from a Type I SMA patient (1-38G) and a Type II individual (1-51N). Both Type I and Type II iPSCs displayed embryonic stem cell morphology and expressed the pluripotency markers OCT4, NANOG and SOX2 (Figures S1A, B). Additional characterization of these iPSCs will be available in a separate manuscript. As controls, two wild-type iPSC lines, BJ-riPS (Warren et al., 2010) and 18a (Boulting et al., 2011), reprogrammed from neonatal foreskin fibroblasts and unaffected adult skin fibroblasts respectively, were used. While the severe Type I (1-38G) cultures express approximately 10% of the full-length SMN protein, Type II (1-51N) cultures retain about 30% of full-length SMN protein compared to wild-type cell lines (Figure S1C). Using established protocols (Amoroso et al., 2013; Yang et al., 2013), we generated MNs from both SMA and wild-type iPSCs (Figure 1A; Supplemental Methods). By day 23 of differentiation, MNs expressing the pan-neuronal marker TUJ1 and MN-specific transcription factors ISL1 and HB9 were formed (Figure 1B). By day 28, some choline acetyltransferase (ChAT) expression was detected in the MN cultures and overall, about 38% of all MNs expressed ISL1 alone, 30% expressed HB9 alone, and 32% of all MNs co-

Author Manuscript Author Manuscript Author Manuscript Author Manuscript

express ISL1 and HB9 (Figure 1C), consistent with the in vivo distribution of single- and double-positive MNs (Amoroso et al., 2013). By day 31, majority (more than 80%) of the ISL1$^+$ and HB9$^+$ MNs also co-express ChAT (Figures 1D–F), an indication of MN maturity.

To reveal disease phenotypes associated with SMA iPSC-derived MNs (Corti et al., 2012; Ebert et al., 2009), we measured basal MN survival by counting ISL1$^+$, HB9$^+$ and ChAT$^+$ MNs from day 28, where ChAT expression was observed (Figure 1D), to day 31. To eliminate dividing progenitors that could give rise to new MNs over this time, cytosine arabinoside (AraC) treatment was included from day 18 to day 23 (Figure 1A). By day 31, a significant decrease in MN survival was observed in the SMA cultures compared to the wild-type MNs (Figures 1G–J). We found both ISL1$^+$ and HB9$^+$ MNs were vulnerable in SMA iPSC-derived cultures, with approximately 50% of Type I MNs, and 40% of Type II MNs lost during the 3-day period while only an insignificant 20% of wild-type MNs were lost during that time (Figures 1G–J). Of note, and percentage of non-MNs, regardless of genotype, remained largely unchanged during this time (Figure S1D), recapitulating a key feature of the disease where selective MN death occurs.

Next, to assess the degree of cell death by apoptosis, immunostaining of cleaved Caspase-3 (cCASP3) was performed at day 28 and this revealed increased apoptosis in SMA MN cultures compared to wild-type cultures, with approximately 20% of Type I, 10% of Type I and 5% of wild-type MNs stained positive for cCASP3 (Figure S1E, F). Supporting our previous observations that both ISL1$^+$ and HB9$^+$ MNs are equally affected in SMA, we found the percentages of apoptotic ISL1$^+$HB9$^-$ MN, ISL1$^-$HB9$^+$ and ISL1$^+$HB9$^+$ MNs to be similar (Figures S1G). Notably, apoptotic rates of non-MNs in wild-type and SMA cultures were low and indistinguishable (approximately 6.5% cCASP3$^+$ISL1$^-$ cells) (Figure S1H). To further ascertain that SMA MN cultures are less viable *in vitro*, we determined the soma size of MNs (Figures 1K, L). While both wild-type and SMA MNs have similar cell body sizes in the range of 220 μm^2 at day 23 (Figure 1L), SMA MNs are significantly smaller (decreasing to approximately 180 μm^2) by day 31 (Figures 1L, M). We also measured soma sizes of apoptotic cCASP3$^+$ MNs and found that they were indeed much smaller than healthy cCASP3$^-$ MNs, measuring 165 μm^2 regardless of whether they are wild-type or SMA (Figure 1M). As soma size is an indication of overall neuronal health, the presence of smaller MNs, even amongst the non-apoptotic MNs, appears to be a disease phenotype associated with SMA.

RNA sequencing of FACS-purified MNs reveals MN-specific changes

Since MNs account for only about 20% of all cells in iPSC-derived cultures, and differentiation efficiencies vary from cell line to cell line, gene expression analysis of whole unpurified cultures will mask important MN-specific events. However, since surface marker purification methods for MNs were unavailable, we used the MARIS (method for analysis of RNA following intracellular sorting) technique (Hrvatin et al., 2014) to obtain a pure HB9$^+$ MN population from day 31 cultures, as the transcription factor HB9 is one of the more specific markers for human MNs (Amoroso et al., 2013). Briefly, cultures were digested into single cells, fixed in paraformaldehyde, and incubated with a specific HB9 antibody in a mild permeabilization/blocking buffer before flow cytometry. Cells marked positive for HB9

Author Manuscript Author Manuscript Author Manuscript Author Manuscript

were then collected (Figure 2A). Total RNA extracted from these FACS-sorted HB9$^+$ cells remained intact (Figure 2B), and qPCR validation confirmed high enrichment of the *HB9* mRNA in the sorted fraction. In addition, the MN markers *ISL1* and *ChAT* were significantly enriched, while non-MN markers, such as *LMX1a* and *S100B*, were significantly depleted in our purified MN RNA samples (Figure 2C). Therefore, to identify cellular pathways that are dysregulated specifically in SMA MNs, we performed massively parallel RNA-sequencing to measure global gene expression of HB9$^+$ purified MNs from SMA and wild-type samples.

SMA MNs display elevated levels of endoplasmic reticulum stress

RNA-sequencing of purified wild-type and Type I SMA MNs revealed 911 differentially expressed mRNAs (fold change cutoff = 1.5; p-value < 0.01), of which 740 were upregulated and 171 downregulated in SMA MNs (Figure 2D; Table S1). To investigate cellular pathways that are modified in SMA MNs, we performed Gene Set Enrichment Analysis (GSEA) (Subramanian et al., 2005), and identified 81 gene sets that were significantly induced in SMA MNs (Normalized Enrichment Score or NES > 1.5) relative to wild-type MNs. Gene sets that were enriched in SMA MNs include terms related to apoptosis (Figure 2E), which we expected from the MN viability studies (Figures S1E–G). We also found that gene sets related with endoplasmic reticulum (ER) stress, such as association of the chaperonin complex TRiC/CCT with target proteins, protein folding and the ER/ phagosome pathway, were enhanced in SMA MNs (Figure 2E). Conversely, we observed depletion of specific gene sets in SMA MNs, including gene sets associated with extracellular matrix, neurite outgrowth and ion channels (Figure 2E), all of which are important in neuronal function, synaptogenesis and the development of the neuromuscular junction (Singhal and Martin, 2011).

Since the pathology of SMA has not been previously linked to unfolded proteins and protein aggregates, we wondered about the relationship between SMN and the ER stress pathway. To expand upon the finding that the unfolded protein response (UPR) and the ER stress pathway are associated with SMA MNs, we further analyzed our RNA-seq results and identified the upregulation of numerous heat shock proteins (HSPA4L, HSPB11, HSP90AB1, DNAJC12, DNAJC18, DNAJC24, HSBP1, DNAJA2), prefoldin subunits (PFDN4, PFDN5, PFDN6), chaperonin subunits (CCT3, CCT4, CCT5, CCT6A, CCT7, CCT8), as well as protein disulfide isomerases that modulate protein folding (PDIA3, PDIA6) in the Type I SMA MNs (Figure 2F), suggesting the activation of the UPR pathway in these MNs.

To confirm upregulation of UPR genes in SMA MNs, RT-qPCR was performed on FACS-purified HB9$^+$ MNs from wild-type (18a and BJ-riPS) and SMA cell lines (1-38G and 1-51N). We saw significant upregulation of the UPR target genes *BiP* (~2.3-fold), spliced XBP1 or *sXBP1* (between 2- to 3.2-fold) and *ATF6* (> 2-fold) in both Type I and II MNs compared to wild-type MNs, with the more severe Type I MNs generally showing a bigger-fold increase. Elevated levels of *IRE1*, *PERK*, *CHOP* and *CASP3* were observed only in the Type I (1-38G) MNs (Figure 3A), suggesting that these undergo more chronic ER stress leading to greater activation of the pro-apoptotic branches of the UPR pathway.

Author Manuscript Author Manuscript Author Manuscript Author Manuscript

In addition, the gene expression profiles of ISL1$^+$ MNs from the wild-type and SMA cell lines were also analyzed. ISL1$^+$ MNs were highly enriched for MN markers (Figure S2A), similar to that observed for HB9$^+$ MNs (Figure 2C). Higher expression levels of UPR markers *BiP* (~2-fold), *sXBP1* (between 2- to 4-fold) and *ATF6* (~2.1-fold) were also observed (Figure S2B). Just as was observed in the purified HB9$^+$ MNs, Type I ISL1$^+$ MNs generally expressed higher levels of ER stress genes. Importantly, these changes in gene expression were not observed when whole unpurified cultures were analyzed, confirming that these are MN-specific changes in SMA (Figure S2C), and underscores the importance of purifying MNs for transcriptome analysis.

To expand upon our findings based on transcriptome analysis, we then performed a series of immunostaining experiments to measure the ER stress response in MNs and other non-MN cells in the day 31 cultures, by quantifying levels of the nuclear transcription factors ATF6 and ATF4. Upon induction of ER stress, ATF6, which is normally sequestered in the ER membrane, is cleaved to give a truncated 50 kDa protein that translocates to the nucleus to activate downstream UPR genes such as ER chaperones and folding catalysts that promote protein folding (Hetz, 2012). We found that nuclear ATF6 intensity in MNs was consistently higher than in non-MNs in all of the cultures (Figure 3B), re-affirming that MNs undergo more basal ER stress than other cells in culture (Kiskinis et al., 2014). More importantly, ISL1$^+$ MNs from SMA cultures (1-38G and 1-51N) show significantly stronger nuclear ATF6 intensity compared to wild-type MNs, with the Type I (1-38G) MNs having 150% more nuclear ATF6 ($p = 0.0039$) and the Type II (1-51N) MNs having 60% more nuclear ATF6 ($p = 0.0047$) compared to the wild-type MNs (Figure 3B). Non-MNs (ISL1$^-$ cells) from the SMA cultures also show increased nuclear ATF6 intensity compared to wild-type controls, although this difference is smaller (Figure 3B), suggesting a MN-selective sensitivity to low SMN levels.

Next, we measured the percentage of cells that express ATF4, a transcription factor activated by the PERK pathway of the UPR (Hetz, 2012). Analysis of day 31 cultures revealed a significant increase in ATF4-expressing cells in SMA cultures (more than 5-fold increase, $p = 0.008$) compared to controls. In addition, approximately 36% of 1-38G MNs also co-express ATF4 while 13% of 1-51N MNs are ATF4$^+$, compared to less than 5% in the wild-type MNs (Figure 3C). Collectively, the transcriptome analysis of purified MNs, as well as quantitative ATF6 and ATF4 immunostaining data, confirm that SMA MNs exhibit the signature of high ER stress levels, with the Type I MNs being the most affected.

ER stress increases in mature MNs, but is not caused by apoptosis

We next investigated if there is a relationship between MN maturity and ER stress and concomitantly, cell death. We performed immunostaining experiments at 3 distinct time points of MN differentiation and maturation (days 23, 28 and 31) and revealed that percentage of ATF4$^+$ MNs increased in SMA MNs, but not wild-type MNs over time (Figures 3D). At day 28, there were significantly more Type I SMA MNs expressing ATF4 (15% compared to < 1% in wild-type MNs), and a similar percentage stained positive for cCASP3. By day 31, percentage of ATF4$^+$ Type I MNs increased to 28%, and ATF4$^+$ Type II MNs increased significantly to 17%, while less than 1% of wild-type MNs are ATF4$^+$

Author Manuscript Author Manuscript Author Manuscript Author Manuscript

(Figure 3D). A similar trend for cCASP3$^+$ apoptotic MNs followed, with increasing cCASP3$^+$ MNs with time, and the severe Type I MNs most affected (Figure 3E). We also found that of the ATF4$^+$ MNs, a vast majority (~83%) were ChAT$^+$ (Figure 3F), indicating that mature ChAT+ MNs were more likely to undergo ER stress activation.

The observation that Type I MNs, which express the least SMN, have the highest expression levels of UPR genes (Figures 3A–C, S2B) suggests a few possibilities: 1) that low SMN protein triggers ER stress activation or 2) the ER stress response is activated in dying cells regardless of SMN expression levels. First, to determine if the UPR is activated in apoptotic cells, we treated wild-type MN cultures with soluble Fas ligand (FasL) to induce apoptosis through the death receptor signaling pathway (Raoul et al., 1999; Ugolini et al., 2003). A 48-hour treatment with FasL significantly increased apoptotic MNs from 6.2% to 14.8% (Figures S3A, D). However, nuclear ATF6 intensity and percentage of ATF4$^+$ MNs remained unchanged (Figures S3B, C, E, F). In addition, gene expression analysis also confirmed that cells treated with FasL did not affect key UPR genes such as *BiP*, *PERK* and *CHOP* (Figure S3G), indicating that the UPR is not necessarily activated in apoptotic cells.

SMN depletion induces ER stress in a dose-dependent manner

Next, to investigate the relationship between SMN and ER stress, we performed small-interfering RNA (siRNA)-mediated knockdown of SMN in wild-type MNs. By transfecting different amounts of siRNAs targeting the *SMN* mRNA, we were able to achieve varying degrees of SMN knockdown (Figures 3G, H). By qPCR, the largest SMN knockdown, si-SMN (20 pmol), resulted in the greatest induction of UPR target genes compared to a non-targeting siRNA (si-NT), whereas the least efficient SMN knockdown, si-SMN (5 pmol), caused only a slight increase (less than two-fold) in *ATF6*, *IRE1* and *CHOP* mRNA (Figure 3G). Similarly, increased levels of the 50 kDa cleaved ATF6 protein were detected in the si-SMN (10 pmol) and si-SMN (20 pmol) conditions, while the pro-apoptotic factor CHOP was induced only in the si-SMN (20 pmol) condition (Figure 3H). More importantly, SMN RNAi led to significantly higher nuclear ATF6 levels in the ISL1$^+$ MNs in a dose-dependent manner (Figure 3I). The percentage of ATF4$^+$ cells also increased upon SMN RNAi, with 70% of MNs co-expressing ATF4 in the severe si-SMN (20 pmol) condition, compared with 25% of ATF4$^+$ MNs in si-SMN (10 pmol) treatment and 6% in the si-NT control (Figure 3J). These results highlight that loss of SMN activates the ER stress pathway in a dose-dependent manner and affects MNs more than other cell types.

SMN overexpression reduces ER stress in SMA MNs

We then performed the reciprocal experiment where we investigated if overexpression of full-length SMN protein would alleviate the ER stress response in SMA MNs. Using an inducible lentiviral system to overexpress the full-length SMN cDNA, we were able to increase SMN protein expression in both Types I and II SMA MNs (Figure 4A). After 3 days, Types I and II MNs express 2.6- and 3.2-fold more SMN protein as detected by immunostaining (Figures 4B, C). Increasing SMN protein in Type I SMA cultures significantly reduced nuclear ATF6 levels in the HB9$^+$, ISL1$^+$ and ChAT$^+$ MN populations but not in the non-MNs (Figure 4D). Reduction in the expression of key UPR markers were also detected with increased SMN expression in SMA MNs (Figures 4E, F). Additionally,

Author Manuscript Author Manuscript Author Manuscript Author Manuscript

percentage of ATF4$^+$ MNs reduced significantly from 21.4% to 12.9% in Type I cultures, and from 10.5% to 4.4% in Type II cultures (Figures 4G, H), further supporting our findings that the UPR pathway acts downstream of SMN. Collectively, the gene perturbation studies (Figures 3, 4) reveal that loss of SMN results in the induction of ER stress in MNs, and increasing SMN expression relieves ER stress in SMA cultures.

Changes in splicing patterns of ER chaperone DNAJC10 in SMA MNs

Since SMN is an RNA-binding protein that functions in the assembly of spliceosomes and modulate alternative splicing (Zhang et al., 2008), we wondered if the elevated ER stress phenotype associated with SMA is due to aberrant splicing of mRNA transcripts. To this end, we analyzed our RNA-seq data for differential splicing events and found 112 significant changes in splicing in our purified HB9$^+$ MN population (Table S2). From the RNA-seq, we found that DNAJC10, an important ER chaperone that maintains normal proteostasis (Ushioda et al., 2008), showed significant splicing changes in SMA MNs (Figure S4A). Importantly, Dnajc10 was also previously identified to be abnormally spliced in SMA mice (Zhang et al., 2008). Human DNAJC10 exists as 5 isoforms; with 2 protein-coding mRNAs, and 3 pseudogene transcripts (Figure 5A, S4A). To investigate the splicing of DNAJC10 in wild-type and SMA MNs, we designed qPCR primers spanning different regions of the DNAJC10 gene, with one pair of primers detecting the pseudogenes, and the other detecting all five isoforms, since specific primers against the protein-coding mRNAs could not be designed (Figure 5A). By qPCR, we found that while total (protein-coding mRNAs and pseudogene RNAs) *DNAJC10* transcript levels stayed the same, *DNAJC10-pseudogene* levels increased in purified SMA MNs compared to wild-type MNs (Figures 5B, C). This suggested that *DNAJC10* protein-coding mRNAs were reduced and since pseudogenes are non-coding, this resulted in reduction of DNAJC10 protein levels in SMN-deficient MNs (Figure 5D). To confirm that SMN is required for the production of *DNAJC10* mRNAs rather than pseudogene RNAs, we evaluated splicing by qPCR upon overexpression of SMN in Type I MN cultures (Figure 4A), and found that pseudogene RNA levels were indeed significantly reduced upon SMN overexpression (Figure 5E).

Interestingly, loss of DNAJC10 has been recently linked to neurodegeneration in animal models (Munoz-Lobato et al., 2014), and we wondered if the reduction of DNAJC10 protein could contribute to ER stress and MN death, as was the case in SMA MNs. We then performed siRNA-mediated knockdown of DNAJC10 in wild-type MN cultures (Figure 5F), which resulted in elevated ER stress marker expression (Figure 5F), along with increased percentage of ATF4$^+$ MNs in DNAJC10-depleted cultures compared to the non-silencing siRNA control (Figure 5G). There was also a significant 25% reduction of MNs (Figure 5H), indicating that reduction of DNAJC10 protein led to increased ER stress and contributes to an accelerated MN death phenotype. Moreover, in the SMAΔ7 mouse model, western blot of spinal cord tissues of mutant animals revealed less DNAJC10 protein compared to the wild-type animals (Figure S4B, D), furthering supporting the role of SMN in regulating DNAJC10 protein levels.

Author Manuscript Author Manuscript Author Manuscript Author Manuscript

SMA MNs are more sensitive to exogenous ER stress

Since SMA MNs already have a high basal level of ER stress signaling, we investigated the possibility that SMA MNs would be more sensitive to exogenous ER stressors compared to wild-type MNs. To achieve this, we treated our iPSC-derived MN cultures for 18 hours with 10 μM tunicamycin, a compound that blocks N-linked glycosylation of nascent proteins (DuRose et al., 2006). We observed ~20% decrease in total cell number upon tunicamycin treatment, regardless of genotype (Figures S5A, B). However, SMA MNs are more vulnerable to tunicamycin stress (55% Type I MN loss, $p = 0.034$, and 50% Type II MN loss, $p = 0.042$) compared to wild-type cultures (~38% MN loss) (Figure S5B). Notably, the percentage of SMA and wild-type non-MNs remained unchanged after tunicamycin treatment (Figure S5C). This suggests that the MN degenerative phenotype in SMA is in part contributed by a MN-specific sensitivity to ER stress that is exacerbated by loss of SMN.

Small molecule inhibitors of ER stress rescue SMA MNs without increasing SMN protein

The discovery that SMA MNs are hyper-sensitive to ER stress led us to investigate if inhibition of the ER stress pathway would prevent the degeneration of SMA MNs. To this end, we first performed RNAi experiments where components of the ER stress pathway were depleted and the effects on MN survival were analyzed. ATF6, XBP1, and the ATF4-activated transcription factor CHOP were significantly depleted by siRNAs in MN cultures (Figures S5D–G). In particular, knockdown of ATF6 resulted in decreased nuclear ATF6 levels in SMA MNs (Figure S5G). Perturbation of the ER stress components by RNAi led to between 30% to 50% MN survival in 1-51N MNs (Figure S5H). In the more severe SMA Type I culture, knockdown of ATF6 or XBP1 led to approximately 30% increase in MNs, while knockdown of CHOP increased MN survival by 80% (Figure S5I).

Additionally, we treated iPSC-derived MN cultures with known small molecule inhibitors of ER stress (Table S3): 4-phenylbutyrate (PBA), Kifunensine (KIF), Salubrinal (SAL), Guanabenz (GUA) and GSK2606414 (GSK) at empirically determined doses (Figure S6). We then assessed MN survival and stress response after three days of small molecule treatment (Figure 6A). We found that inhibition of the ER stress pathway by these various small molecules led to greater MN survival compared to DMSO treatment in SMA Type I and II cultures, with SAL and GUA consistently more effective than the other ER stress inhibitors in promoting MN survival (Figure 6B, C). In addition, treatment of wild-type cultures with ER stress inhibitors marginally enhanced MN survival, albeit insignificantly (Figure 6D). This observation re-affirms that the ER stress hyper-sensitivity phenotype is specific to SMA MNs.

Importantly, the small molecule ER stress inhibitors did not increase cellular SMN protein in SMA Type I and II MN cultures (Figure 6E), although PBA led to approximately 25% increase in full-length *SMN* mRNA (Figure S5J) as has been previously reported (Andreassi et al., 2004). Rather, these small molecules, particularly SAL, GUA and GSK resulted in attenuation of the UPR pathway including downregulation of the pro-apoptotic protein CHOP (Figure 6E), reduced XBP1 splicing (Figure 6F), and decreased nuclear ATF6 intensity (Figure 6G). Consequently, the percentage of MNs co-expressing cleaved Caspase-3 also decreased (Figure 6H). This indicates that inhibition of ER stress is sufficient

Author Manuscript Author Manuscript Author Manuscript Author Manuscript

to prevent MN degeneration in SMA cultures, without needing to elevate SMN protein levels.

Treatment of SMA motor neurons with ER stress inhibitors reverses disease phenotype

We also measured soma sizes of $ISL1^+/TUJ1^+$ MNs treated with ER stress inhibitors, and compared that to cultures treated with DMSO. While DMSO-treated Type I MNs measured approximately 180 μm^2 (Figures 1L, 6I), treatment with ER stress inhibitors increased soma sizes significantly by at least 10 μm^2. We noticed that SAL and GUA, small molecules that were most effective in rescuing SMA MNs, also had MNs with largest somas (approximately 205 μm^2, $p < 0.01$). Similar results were also obtained using Type II SMA 1-51N motor neurons, where SAL and GUA were also most effective at increasing soma sizes ($p < 0.05$) (Figures 6J, K). Notably, SAL- and GUA-treated SMA MNs measure approximately 210 μm^2, very similar to wild-type MNs (measuring approximately 220 μm^2) (Figure 1L).

GUA alleviates ER stress and preserves ventral horn MNs in SMAΔ7 mice

Next, we questioned if elevated ER stress is also observed in the SMAΔ7 mice and whether ER stress inhibition would promote SMA MN survival *in vivo*. The SMAΔ7 mouse displays a relatively severe decrease in average lifespan concurrent with early impairment of motor behavior correlating with fewer spinal MNs (Le et al., 2005). By immunoblotting, we compared expression of UPR markers of spinal cords from late symptomatic SMAΔ7 mice at post-natal day (PND) 12 to their wild-type (WT) littermates. Consistent with *in vitro* results, we observed increased levels of cleaved Atf6 and Chop in the SMAΔ7 spinal cords (Figure 7A), confirming elevated ER stress in SMA MNs *in vivo*. We then analyzed the effect of ER stress inhibition on the SMAΔ7 mice.

In vitro analyses indicate that GUA, an inhibitor of eIF2α dephosphorylation (Tsaytler et al., 2011), was most effective in the rescue of SMA MNs (Figure 6). Moreover, GUA penetrates the blood-brain-barrier (Meacham et al., 1981), making it an ideal ER stress inhibitor to test *in vivo*. To investigate the effects of GUA treatment on SMA mice, we administered 4 mg/kg GUA by subcutaneous injections (Tribouillard-Tanvier et al., 2008) into pre-symptomatic PND2 mice twice daily. First, to determine if GUA was able to reduce UPR markers in the spinal cords of SMAΔ7 mice, we performed qPCR and immunoblotting on spinal cord sections from fully symptomatic PND8 mice, after they were treated with either GUA or DMSO. SMAΔ7 mice treated with GUA had significantly higher levels of phospho-eIF2α, confirming that GUA was able to cross the blood-brain-barrier and retain its function in the spinal cords (Figures S4B, C). We found that SMAΔ7 mice that received twice-daily GUA doses had reduced expression of UPR transcripts *Ire1*, *Chop*, *Atf4* and *Pfdn5*, to levels similar in wild-type mice (Figure 7B). Furthermore, GUA-treated SMAΔ7 mice also had about reduced *Caspase-3*, *Caspase-4*, and *Caspase-12* expression similar to wild-type mice (Figure 7C). Importantly, Caspase-4 and Caspase-12 are activated in response to ER stress (Hitomi et al., 2004; Kim et al., 2006; Nakagawa et al., 2000). GUA treatment also led to a 3-fold increase in *ChAT* mRNA compared to DMSO-treated SMA animals. Taken together, the qPCR results suggest that ER stress-mediated apoptosis is inhibited in spinal MNs of GUA-treated SMA mice, possibly leading to MN preservation. Western blot analysis of

Author Manuscript Author Manuscript Author Manuscript Author Manuscript

spinal cord sections confirmed our qPCR results. While GUA does not change Smn protein levels in spinal cords of treated animals, we observed reduced UPR markers cleaved Atf6, Chop, Caspase-4 and Caspase-12, along with an increase in the MNs markers ChAT and Smi-32 in treated animals (Figure 7E).

To confirm the preservation of spinal cord MNs in GUA-treated animals, we analyzed 20 lumbar sections of each PND8 mouse (4–5 animals per condition), representative of the entire lumbar spinal cord, and counted the number of $ChAT^+$ MNs in the ventral horns (Figure 7F). On average, DMSO-treated SMAΔ7 animals have fewer MNs compared to DMSO-treated wild-type animals (13.5 versus 22.7 ChAT+ MNs per 10 μm section; $p = 0.0028$), similar to previous reports (d'Errico et al., 2013; Mentis et al., 2011). Importantly, we observed that GUA treatment increased the number of $ChAT^+$ MNs by an average of 40 (± 5) % in SMAΔ7 animals compared to DMSO-treated animals ($p = 0.034$; Figure 7G), indicating that GUA prevents degeneration of spinal MNs by inhibition of ER stress.

Previous studies have shown that MN soma sizes are significantly smaller in SMAΔ7 mice as early as PND4 (d'Errico et al., 2013), suggesting that MNs are undergoing atrophy and large MNs are lost even when the animals are pre-symptomatic. We also found that DMSO-treated SMAΔ7 MNs were significantly smaller than DMSO-treated wild-type MNs (220 ± 25 μm^2 in SMA and 316 ± 27 μm^2 in WT; $p = 0.0092$). Importantly, $ChAT^+$ MNs of SMAΔ7 animals treated with GUA were larger (296 ± 28 μm^2; $p = 0.0277$), similar to the sizes of wild-type MNs, suggesting the presence of healthier MNs in GUA-treated SMAΔ7 animals (Figure 7H). Consequently, GUA treatment led to an approximately 30% increase in lifespan of SMA animals, from a maximum of 13 days (median = 10 days) to 17 days (median = 13 days) (Figure 7I).

Because of MN loss in SMA mice, denervation of neuromuscular junctions (NMJs) is evident in vulnerable muscle groups (d'Errico et al., 2013; Le et al., 2005). This led to motor deficits in SMA mice that resulted in their inability to right. We measured righting reflex times of DMSO- and GUA-treated mice at PND8 before the mice were sacrificed, and found that GUA treatment significantly reduced righting reflex time of SMA mice (Figure 7J). Analysis of hindlimb muscles of PND8 mice revealed that GUA treatment prevented the denervation of NMJs in SMA mice (Figure 7K), with approximately 60% of hindlimb NMJs remaining innervated compared to 42% of innervated NMJs ($p = 0.0125$) in DMSO-treated SMA mice. Collectively, these results indicate that inhibition of ER stress by GUA led to preservation of spinal MNs *in vivo*, which was accompanied by improvement in lifespan and motor ability of SMAΔ7 mice.

DISCUSSION

Directed differentiation of patient-derived iPSCs holds great promise in understanding neurodegenerative diseases, such as SMA, that affects selective neuronal populations. However, differentiation into specific neuronal subtypes is not always efficient, and gene expression profiling and other types of studies carried out using mixed cultures can mask important cellular events taking place in the neuronal population of interest. Since surface markers specific to MNs and many other types of neurons have not yet been established, we

Author Manuscript Author Manuscript Author Manuscript Author Manuscript

circumvented the MN purification problem by isolating cells based on their unique transcription factor expression for deep transcriptome sequencing.

One of our key findings is that SMA MNs show a hyper-sensitivity to ER stress, and this is caused by increased activation of UPR genes in response to SMN deficiency. This activation is more pronounced in MNs than non-MNs, presumably because MNs already possess basal ER stress signaling (Kiskinis et al., 2014), and additional activation is more likely to surpass the threshold level the cell can withstand without committing apoptosis. We have also identified that abnormal splicing of a key ER chaperone, DNAJC10, contributes in part to the elevated ER stress phenotype observed in SMN-deficient MNs.

Furthermore, our cell culture-based model of SMA accurately predicted *in vivo* results in SMAΔ7 mice. Importantly, we observed increased activation of ER stress markers in spinal cords of SMA mice. GUA, the ER stress inhibitor that was most effective *in vitro*, also preserved MN numbers and size in SMA mice. Notably, we also tested PBA on our SMA iPSC-derived MNs and noticed a lack of efficacy *in vitro*. PBA was previously identified as a drug for clinical trials on SMA patients but failed in Phase II due to a lack of efficacy. This would have been predicted by our cell-culture model system.

As a proof-of-concept that inhibition of ER stress is important for SMA MN survival, SMA mice treated with GUA demonstrated reduced spinal cord UPR marker expression, along with improved spinal MN survival and motor function, and a modest increase in lifespan. Since MNs are particularly susceptible to ER stress, it is unlikely that treatment with drugs like GUA will alleviate all of the systemic defects caused by SMN deficiency. Notably, a prior study showed that increasing SMN in motor neurons alone in a severe SMA mouse model (SMN2$^{+/-}$; *Smn*$^{2B\text{-}Neo/2B\text{-}Neo}$) preserved MNs, but also had a maximum lifespan of 16 days (median = 12 days) (Gogliotti et al., 2012), very similar to what we found in our GUA-treated SMAΔ7 mice that survived for a maximum of 17 days (median = 13 days). Thus, neuroprotection alone, achieved either by reducing ER stress or restoring SMN expression only in MNs, is unlikely to be sufficient to correct all of the defects found in children with SMA. Other studies also indicate that increasing SMN expression in the central nervous system alone (MNs and non-MNs) was able to extend lifespan of SMAΔ7 mice to 30 days (Hua et al., 2011), while restoration of SMN expression to peripheral tissues alone is sufficient for long-term rescue of SMA mice for more than 300 days (Hua et al., 2015; Hua et al., 2011). Taken together, our results support our view that (a) increased ER stress is a pathway that explains why MNs, but not other cells, are affected by low levels of SMN; (b) reducing ER stress does not correct systemic aspects of the SMA phenotype. It will be important to identify pathways that mediate dysfunction seen in other tissues with low levels of SMN.

In conclusion, transcriptome profiling of purified cell populations opens a new avenue for understanding disease mechanisms. Using this strategy, we found ER stress hyperactivity and a hyper-sensitivity phenotype associated with SMA MNs. Small molecule inhibition of ER stress rescued SMA MNs *in vitro* and *in vivo*, with treated mice showing improved motor function and a modest increase in lifespan. Our current work serves as proof-of-principle that targeting disease phenotypes identified *in vitro* using patient iPSCs accurately

Author Manuscript Author Manuscript Author Manuscript Author Manuscript

predicts disease-related outcomes in even *in vivo* and may be used as a strategy to understand other neurodegenerative diseases showing cell type-specific vulnerability.

EXPERIMENTAL PROCEDURES

Human iPSC culture and MN differentiation

Two wild-type human iPSC lines BJ-riPS (Warren et al., 2010) and 18a (Boulting et al., 2011), a Type I SMA patient-specific iPSC line (1-38G), and a Type II SMA iPSC line (1-51N) were routinely cultured on Matrigel-coated dishes in MTeSR media (Stem Cell Technologies). MNs were differentiated as previously described (Amoroso et al., 2013) with slight modifications (Supplemental Methods).

Purification of MNs by MARIS for gene expression analysis

Day 28 MN cultures were dissociated into single cells using Accutase, and fixed in 4% PFA. HB9 antibody (Developmental Studies Hybridoma Bank 81.5C10) was diluted 1:100 in blocking buffer (1% BSA) and 0.2% saponin (Sigma) in PBS supplemented with 50 U/ml Superase.In (Ambion), and incubated with the cell suspension for 3 hours. AlexaFluor-488 conjugated secondary antibody was diluted 1:1000 in blocking buffer, and incubated with the cell suspension. The cells were then washed with DPBS before FACS on BD FACS Aria. Sorted cells were treated with Proteinase K for an hour at 50 °C, before addition of Trizol LS (Invitrogen) for RNA extraction. DNase treatment using Turbo DNA-free (Ambion) was performed to remove contaminating genomic DNA.

mRNA-seq library preparation and sequencing

Illumina mRNA-seq libraries were prepared using the TruSeq RNA kit, using 200 ng of total RNA. Library sequence was carried out on an Illumina MiSeq with four samples from both conditions pooled together with each library sequenced up to depth of ~30 million fragments using a 100bp paired end flow cell. RNA-seq reads were mapped using TopHat version 2.0.9 against the human genome build hg19. Details of the RNA-seq analyses are provided in the Supplemental Methods. The data is available at GEO accession GSE69175.

cDNA synthesis and PCR

Quantitative PCR (qPCR) analyses on cDNA transcribed with High-Capacity cDNA Reverse Transcription kit was performed on the QuantStudio 12K Flex System, using the FAST SYBR Master mix (all from Applied Biosystems), and normalized to *GAPDH* or *ACTB* expression. A list of human primers is provided in Table S4, while mouse primers are listed in Table S5.

RNA interference

MN cultures were seeded at 50,000 cells per well in a 96-well plate. Non-targeting siRNA or siRNA against human SMN (Santa Cruz) were complexed with Lipofectamine RNAiMAX (Invitrogen), following manufacturer's instructions. To enhance knockdown efficiency for a period of seven days, a second transfection was repeated 3 days after the initial transfection.

Author Manuscript Author Manuscript Author Manuscript Author Manuscript

SMN overexpression

The full-length SMN1 cDNA was cloned into the doxycycline-inducible pTRIPZ lentiviral construct (OpenBiosystems), with a puromycin selection marker. The control was an RFP cDNA. Lentiviral particles were made and concentrated. Day 23 MN cultures were infected with either SMN lentiviral paricles or RFP lentiviral particles in the presence of 8 μg/ml polybrene. Puromycin (500 ng/ml) selection and 500 ng/ml doxycycline treatment, where applicable, were pursued for 3 days before the cells were harvested for RNA and protein or fixed for immunostaining (Figure 4A).

Small molecule treatment

Tunicamycin (Calbiochem), Sodium-4-phenylbutyrate (EMD Millipore), Kifunensine (Tocris), Salubrinal (Calbiochem), Guanabenz acetate (Tocris) and GSK2606414 (EMD Millipore) were reconstituted in DMSO and diluted in MN media at the desired concentrations. Sodium-4-phenylbutyrate was used at 2 mM (Qi et al., 2004). For the other compounds, a dose response assay was performed to determine the most effective concentration for *in vitro* experiments (Figure S6).

Immunostaining

Cells were fixed in 4% PFA, permeabilized with 0.1% Triton X-100, and blocked with buffer consisting 5% fetal bovine serum (FBS) and 1% BSA. Primary antibodies used in this study (and their respective dilutions) are as follow: rabbit ISL1 (Abcam ab109517; 1:1000), mouse TUJ1 (Covance MMS-435P; 1:1000), mouse HB9 (DSHB 81.5C10; 1:200), mouse ISL1 (DSHB 39.4D5), mouse SMI-32 (Calbiochem NE-1023; 1:1000), goat ChAT (Millipore AB114P; 1:100), rabbit ATF6 (Abcam ab37149; 1:500), rabbit ATF4 (Cell Signaling #11815; 1:100), rabbit cleaved Caspase-3 (Cell Signaling #9661) and mouse monoclonal SMN (BD Pharmingen; 1:250). Cellular nuclei were counterstained with 0.5 μg/ml DAPI.

Image acquisition and analysis

Fluorescent images were acquired by an automated microscope (PerkinElmer Operetta) at 20x magnification. Image analysis was performed using the Columbus software (PerkinElmer), by first recognizing and outlining cellular nuclei based on DAPI. MNs were identified based on ISL1 expression, and nuclear intensities of ATF6 or ATF4 were measured. Since there is basal expression of nuclear ATF6 in MNs, we measured the relative intensities of average nuclear ATF6 per MN, and normalize the intensity with wild-type cultures. ATF4 is not basally expressed, and we took the intensity cutoff of >150 to define a positive stain.

For soma size analysis, cellular nuclei were identified by DAPI, and the cytoplasmic area surrounding the nucleus was determined based on TUJ1 staining. Soma size area is measured based on the cytoplasmic area surrounding the nucleus, excluding neuronal projections (Figure 1K).

Author Manuscript Author Manuscript Author Manuscript Author Manuscript

Western blot analysis

Cells or tissue sections were lysed in RIPA buffer (Sigma) with protease inhibitor (Roche) and phosphatase inhibitor cocktail (Santa Cruz). Samples containing 25 μg of protein were boiled in Laemmli buffer and resolved on 10% Tris-glycine polyacrylamide gels. Proteins were transferred to PVDF membranes, blocked with 5% milk and incubated overnight with primary antibodies as follow: mouse SMN (BD Pharmingen; 1:1000), rabbit ATF6α (Abcam ab37149; 1:500), mouse CHOP (Santa Cruz sc-7351; 1:100), rabbit GAPDH (Abcam ab9485; 1:2000), rabbit α-tubulin (Abcam ab126165; 1:2000). The blots were then incubated with respective HRP-conjugated antibodies at 1:2000 dilution.

Animals and drug administration

All animal studies were approved by Harvard University Institutional Animal Care and Use Committee and performed in accordance with institutional and federal guidelines. FVB mice were obtained from Charles River Laboratory. The original breeding pair of heterozygous SMNΔ7 mice ($mSmn^{+/-}$;$SMN2^{+/+}$,$SMN\Delta7^{+/+}$) on FVB background were provided by the Jackson Laboratory. Guanabenz was resuspended in DMSO at 10 mg/ml as a stock solution and diluted in 10% (2-Hydroxypropyl)-β-cyclodextrin right before administrating at 4 mg/kg via subcutaneous injections starting at PND2. Animals received doses twice daily (injections 8 hours apart) and were euthanized at PND8. The spinal cords were dissected and cervical regions were homogenized in RIPA buffer for Western blot, lumbar regions were collected for immunostaining and thoracic regions were utilized for RNA expression studies. Hindlimb muscles were dissected and embedded in OCT-sucrose for cryostat sectioning.

Statistical Analyses

In vitro studies were performed in 4 independent experiments (biological replicates), with 6–10 independent wells (technical replicates) unless otherwise stated. Student's t test was performed to assess statistical significance. Throughout the manuscript, * denotes $p < 0.05$, ** denotes $p < 0.01$, *** for $p < 0.001$ and *n.s* denotes a p-value that is not significant. Error bars shown are standard deviation unless otherwise stated.

Supplementary Material

Refer to Web version on PubMed Central for supplementary material.

Acknowledgments

We would like to thank Catherine McGillivary for histology assistance and Erika Norabuena for genotyping of mice. This work is supported by grants from the NINDS (1P01NS066888), the Spinal Muscular Atrophy Foundation, and the Harvard Stem Cell Institute. SYN is a recipient of the A*STAR International Fellowship (Singapore).

References

Amoroso MW, Croft GF, Williams DJ, O'Keeffe S, Carrasco MA, Davis AR, Roybon L, Oakley DH, Maniatis T, Henderson CE, et al. Accelerated high-yield generation of limb-innervating motor neurons from human stem cells. J Neurosci. 2013; 33:574–586. [PubMed: 23303937]

Author Manuscript Author Manuscript Author Manuscript Author Manuscript

Andreassi C, Angelozzi C, Tiziano FD, Vitali T, De Vincenzi E, Boninsegna A, Villanova M, Bertini E, Pini A, Neri G, et al. Phenylbutyrate increases SMN expression in vitro: relevance for treatment of spinal muscular atrophy. Eur J Hum Genet. 2004; 12:59–65. [PubMed: 14560316]

Boulting GL, Kiskinis E, Croft GF, Amoroso MW, Oakley DH, Wainger BJ, Williams DJ, Kahler DJ, Yamaki M, Davidow L, et al. A functionally characterized test set of human induced pluripotent stem cells. Nat Biotechnol. 2011; 29:279–286. [PubMed: 21293464]

Burghes AH, Beattie CE. Spinal muscular atrophy: why do low levels of survival motor neuron protein make motor neurons sick? Nat Rev Neurosci. 2009; 10:597–609. [PubMed: 19584893]

Corti S, Nizzardo M, Simone C, Falcone M, Nardini M, Ronchi D, Donadoni C, Salani S, Riboldi G, Magri F, et al. Genetic correction of human induced pluripotent stem cells from patients with spinal muscular atrophy. Sci Transl Med. 2012; 4:165ra162.

d'Errico P, Boido M, Piras A, Valsecchi V, De Amicis E, Locatelli D, Capra S, Vagni F, Vercelli A, Battaglia G. Selective vulnerability of spinal and cortical motor neuron subpopulations in delta7 SMA mice. PLoS One. 2013; 8:e82654. [PubMed: 24324819]

DuRose JB, Tam AB, Niwa M. Intrinsic capacities of molecular sensors of the unfolded protein response to sense alternate forms of endoplasmic reticulum stress. Mol Biol Cell. 2006; 17:3095–3107. [PubMed: 16672378]

Ebert AD, Yu J, Rose FF Jr, Mattis VB, Lorson CL, Thomson JA, Svendsen CN. Induced pluripotent stem cells from a spinal muscular atrophy patient. Nature. 2009; 457:277–280. [PubMed: 19098894]

Foust KD, Wang X, McGovern VL, Braun L, Bevan AK, Haidet AM, Le TT, Morales PR, Rich MM, Burghes AH, et al. Rescue of the spinal muscular atrophy phenotype in a mouse model by early postnatal delivery of SMN. Nat Biotechnol. 2010; 28:271–274. [PubMed: 20190738]

Gogliotti RG, Quinlan KA, Barlow CB, Heier CR, Heckman CJ, Didonato CJ. Motor neuron rescue in spinal muscular atrophy mice demonstrates that sensory-motor defects are a consequence, not a cause, of motor neuron dysfunction. J Neurosci. 2012; 32:3818–3829. [PubMed: 22423102]

Hetz C. The unfolded protein response: controlling cell fate decisions under ER stress and beyond. Nat Rev Mol Cell Biol. 2012; 13:89–102. [PubMed: 22251901]

Hitomi J, Katayama T, Eguchi Y, Kudo T, Taniguchi M, Koyama Y, Manabe T, Yamagishi S, Bando Y, Imaizumi K, et al. Involvement of caspase-4 in endoplasmic reticulum stress-induced apoptosis and Abeta-induced cell death. J Cell Biol. 2004; 165:347–356. [PubMed: 15123740]

Hrvatin S, Deng F, O'Donnell CW, Gifford DK, Melton DA. MARIS: method for analyzing RNA following intracellular sorting. PLoS One. 2014; 9:e89459. [PubMed: 24594682]

Hua Y, Liu YH, Sahashi K, Rigo F, Bennett CF, Krainer AR. Motor neuron cell-nonautonomous rescue of spinal muscular atrophy phenotypes in mild and severe transgenic mouse models. Genes Dev. 2015; 29:288–297. [PubMed: 25583329]

Hua Y, Sahashi K, Rigo F, Hung G, Horev G, Bennett CF, Krainer AR. Peripheral SMN restoration is essential for long-term rescue of a severe spinal muscular atrophy mouse model. Nature. 2011; 478:123–126. [PubMed: 21979052]

Kim SJ, Zhang Z, Hitomi E, Lee YC, Mukherjee AB. Endoplasmic reticulum stress-induced caspase-4 activation mediates apoptosis and neurodegeneration in INCL. Hum Mol Genet. 2006; 15:1826–1834. [PubMed: 16644870]

Kiskinis E, Sandoe J, Williams LA, Boulting GL, Moccia R, Wainger BJ, Han S, Peng T, Thams S, Mikkilineni S, et al. Pathways Disrupted in Human ALS Motor Neurons Identified through Genetic Correction of Mutant SOD1. Cell Stem Cell. 2014

Le TT, Pham LT, Butchbach ME, Zhang HL, Monani UR, Coovert DD, Gavrilina TO, Xing L, Bassell GJ, Burghes AH. SMNDelta7, the major product of the centromeric survival motor neuron (SMN2) gene, extends survival in mice with spinal muscular atrophy and associates with full-length SMN. Hum Mol Genet. 2005; 14:845–857. [PubMed: 15703193]

Meacham RH, Chiang ST, Kick CJ, Sisenwine SF, Jusko WJ, Ruelius HW. Pharmacokinetic disposition of guanabenz in the rhesus monkey. Drug Metab Dispos. 1981; 9:509–514. [PubMed: 6120807]

Author Manuscript Author Manuscript Author Manuscript Author Manuscript

Mentis GZ, Blivis D, Liu W, Drobac E, Crowder ME, Kong L, Alvarez FJ, Sumner CJ, O'Donovan MJ. Early functional impairment of sensory-motor connectivity in a mouse model of spinal muscular atrophy. Neuron. 2011; 69:453–467. [PubMed: 21315257]

Munoz-Lobato F, Rodriguez-Palero MJ, Naranjo-Galindo FJ, Shephard F, Gaffney CJ, Szewczyk NJ, Hamamichi S, Caldwell KA, Caldwell GA, Link CD, et al. Protective role of DNJ-27/ERdj5 in Caenorhabditis elegans models of human neurodegenerative diseases. Antioxid Redox Signal. 2014; 20:217–235. [PubMed: 23641861]

Nakagawa T, Zhu H, Morishima N, Li E, Xu J, Yankner BA, Yuan J. Caspase-12 mediates endoplasmic-reticulum-specific apoptosis and cytotoxicity by amyloid-beta. Nature. 2000; 403:98–103. [PubMed: 10638761]

Qi X, Hosoi T, Okuma Y, Kaneko M, Nomura Y. Sodium 4-phenylbutyrate protects against cerebral ischemic injury. Mol Pharmacol. 2004; 66:899–908. [PubMed: 15226415]

Raoul C, Henderson CE, Pettmann B. Programmed cell death of embryonic motoneurons triggered through the Fas death receptor. J Cell Biol. 1999; 147:1049–1062. [PubMed: 10579724]

Singhal N, Martin PT. Role of extracellular matrix proteins and their receptors in the development of the vertebrate neuromuscular junction. Dev Neurobiol. 2011; 71:982–1005. [PubMed: 21766463]

Subramanian A, Tamayo P, Mootha VK, Mukherjee S, Ebert BL, Gillette MA, Paulovich A, Pomeroy SL, Golub TR, Lander ES, et al. Gene set enrichment analysis: a knowledge-based approach for interpreting genome-wide expression profiles. Proc Natl Acad Sci U S A. 2005; 102:15545–15550. [PubMed: 16199517]

Tribouillard-Tanvier D, Beringue V, Desban N, Gug F, Bach S, Voisset C, Galons H, Laude H, Vilette D, Blondel M. Antihypertensive drug guanabenz is active in vivo against both yeast and mammalian prions. PLoS One. 2008; 3:e1981. [PubMed: 18431471]

Tsaytler P, Harding HP, Ron D, Bertolotti A. Selective inhibition of a regulatory subunit of protein phosphatase 1 restores proteostasis. Science. 2011; 332:91–94. [PubMed: 21385720]

Ugolini G, Raoul C, Ferri A, Haenggeli C, Yamamoto Y, Salaun D, Henderson CE, Kato AC, Pettmann B, Hueber AO. Fas/tumor necrosis factor receptor death signaling is required for axotomy-induced death of motoneurons in vivo. J Neurosci. 2003; 23:8526–8531. [PubMed: 13679421]

Ushioda R, Hoseki J, Araki K, Jansen G, Thomas DY, Nagata K. ERdj5 is required as a disulfide reductase for degradation of misfolded proteins in the ER. Science. 2008; 321:569–572. [PubMed: 18653895]

Warren L, Manos PD, Ahfeldt T, Loh YH, Li H, Lau F, Ebina W, Mandal PK, Smith ZD, Meissner A, et al. Highly efficient reprogramming to pluripotency and directed differentiation of human cells with synthetic modified mRNA. Cell Stem Cell. 2010; 7:618–630. [PubMed: 20888316]

Yang YM, Gupta SK, Kim KJ, Powers BE, Cerqueira A, Wainger BJ, Ngo HD, Rosowski KA, Schein PA, Ackeifi CA, et al. A small molecule screen in stem-cell-derived motor neurons identifies a kinase inhibitor as a candidate therapeutic for ALS. Cell Stem Cell. 2013; 12:713–726. [PubMed: 23602540]

Zhang Z, Lotti F, Dittmar K, Younis I, Wan L, Kasim M, Dreyfuss G. SMN deficiency causes tissue-specific perturbations in the repertoire of snRNAs and widespread defects in splicing. Cell. 2008; 133:585–600. [PubMed: 18485868]

Author Manuscript Author Manuscript Author Manuscript Author Manuscript

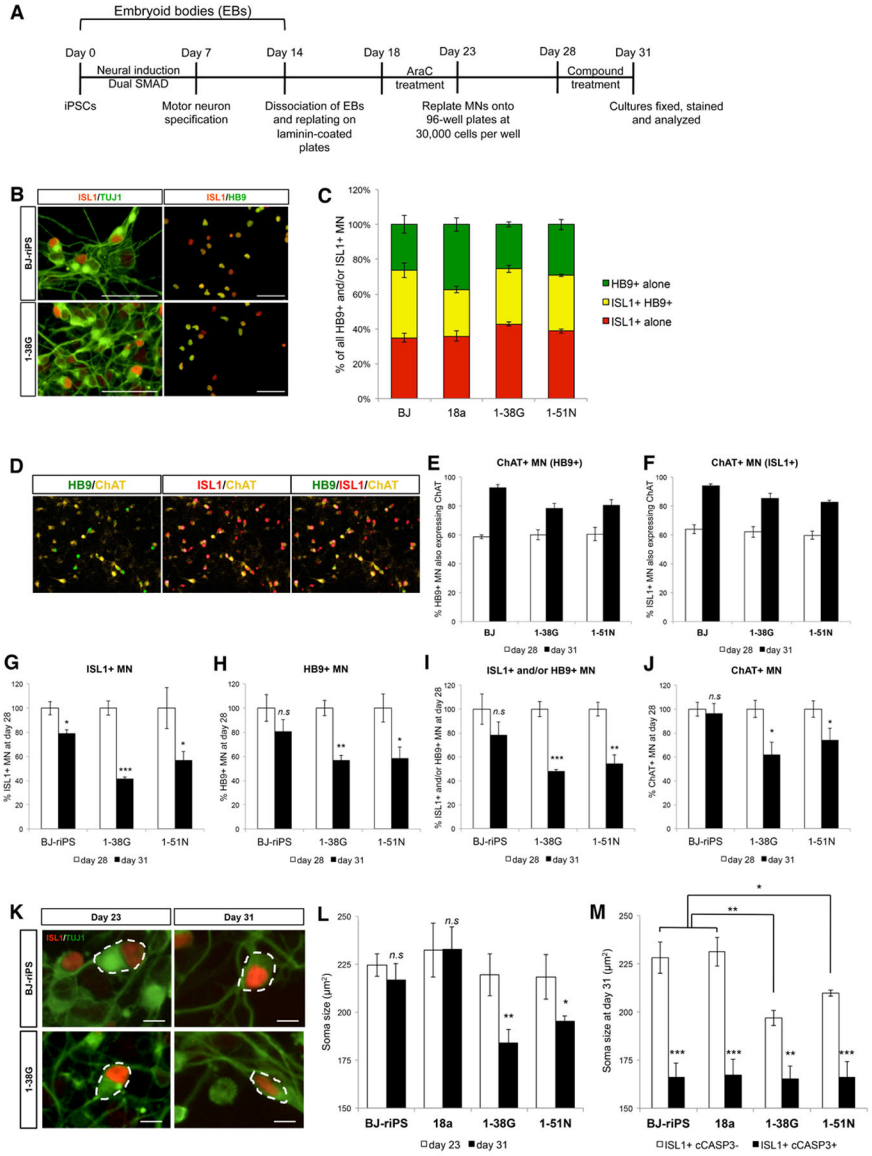

Figure 1. MNs differentiated from SMA-iPSCs show increased apoptosis and have smaller cell bodies. (See also Figure S1)

(A) Differentiation scheme of iPSCs to MNs in 31 days.

(B) MN cultures at day 23, showing that both wild-type (BJ-riPS) and SMA Type I (1-38G) iPSCs differentiate into MNs expressing ISL1 and TUJ1. Many $ISL1^+$ cells also co-express HB9, another MN transcription factor. The scale bar indicates 50 μm.

(C) Percentage overlap between ISL1 and HB9 expression in MNs assessed by immunostaining. The percentages of $ISL1^+/HB9^-$, $ISL1^+/HB9^+$ and $ISL1^-/HB9^+$ MNs were similar between wild-type and SMA iPSC-derived cultures.

(D) Immunostaining showing $HB9^+$ and/or $ISL1^+$ co-expressing ChAT at day 28.

(E) Quantification of $HB9^+$ MNs co-expressing ChAT at days 28 and 31.

(F) Quantification of $ISL1^+$ MNs co-expressing ChAT at days 28 and 31.

Author Manuscript Author Manuscript Author Manuscript Author Manuscript

(G–J) Quantification of respective $ISL1^+$, $HB9^+$, $ISL1^+$ and/or $HB9^+$ and $ChAT^+$ MN numbers from wild-type (BJ-riPS), SMA Type I (1-38G) and SMA Type II (1-51N) cultures at days 28 and 31. Numbers are shown as percentages normalized to respective MN count at day 28.

(K) Representative images of BJ-riPS and 1-38G-derived MNs co-stained with ISL1 and TUJ1 at day 23 and day 31. The white-dotted circumference represents the measured soma sizes.

(L) Measurements of $ISL1^+$ MN soma sizes at day 23 and day 31. At day 23, soma sizes of wild-type and SMA MNs were similar – between 210 μm^2 and 230 μm^2. By day 31, wild-type MNs remained in size while SMA MNs were significantly smaller.

(M) Measurements of healthy ($ISL1^+cCASP3^-$) MN soma sizes and apoptotic ($ISL1^+cCASP3^+$) MN soma sizes at day 31 showing that apoptotic MNs were significantly smaller, regardless of genotype (about 165 μm^2), and that non-apoptotic SMA MNs remain smaller compared to wild-type counterparts.

Author Manuscript Author Manuscript Author Manuscript Author Manuscript

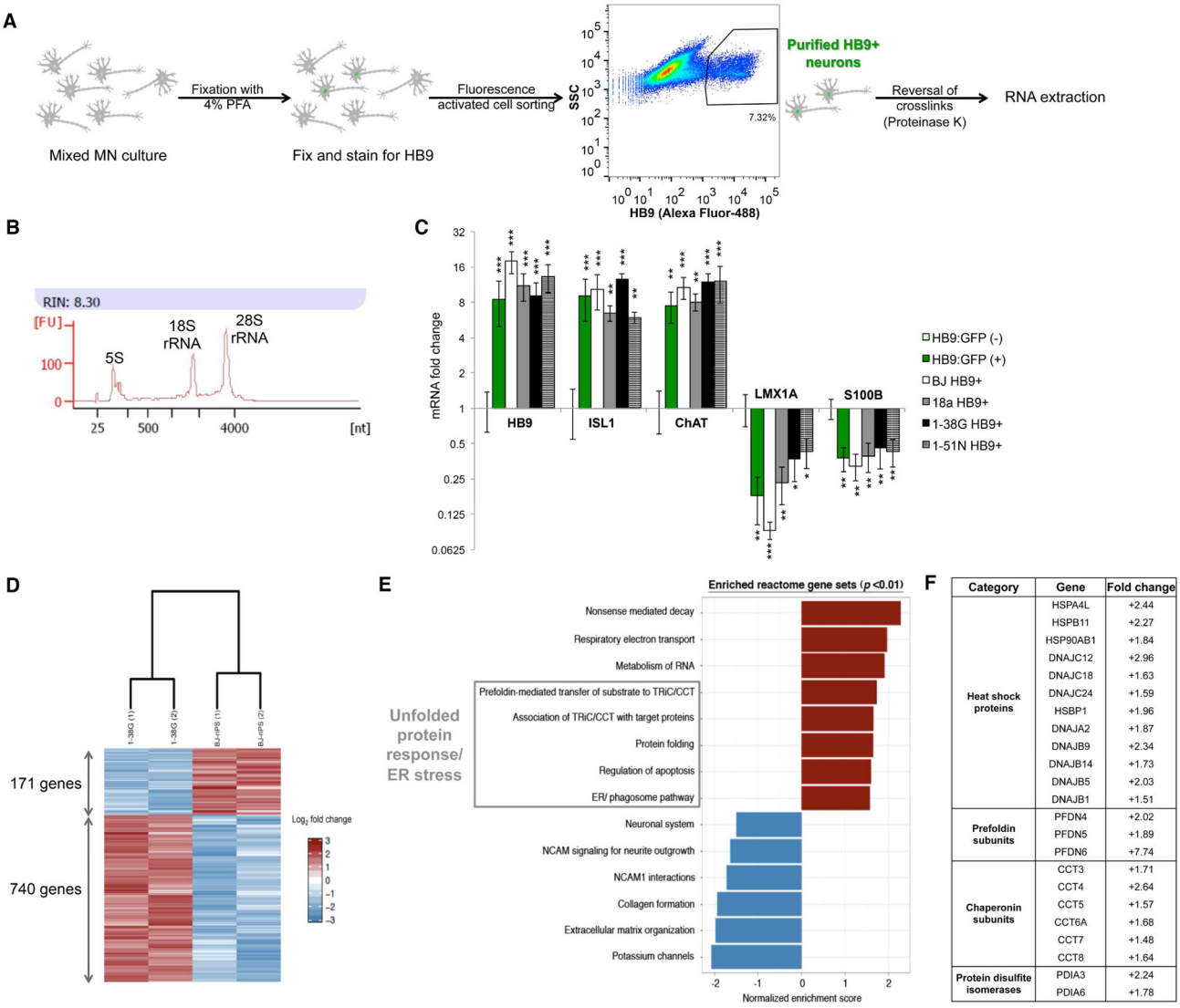

Category	Gene	Fold change
Heat shock proteins	HSPA4L	+2.44
	HSPB11	+2.27
	HSP90AB1	+1.84
	DNAJC12	+2.96
	DNAJC18	+1.63
	DNAJC24	+1.59
	HSBP1	+1.96
	DNAJA2	+1.87
	DNAJB9	+2.34
	DNAJB14	+1.73
	DNAJB5	+2.03
	DNAJB1	+1.51
Prefoldin subunits	PFDN4	+2.02
	PFDN5	+1.89
	PFDN6	+7.74
Chaperonin subunits	CCT3	+1.71
	CCT4	+2.64
	CCT5	+1.57
	CCT6A	+1.68
	CCT7	+1.48
	CCT8	+1.64
Protein disulfite isomerases	PDIA3	+2.24
	PDIA6	+1.78

Figure 2. Genome-wide RNA-sequencing of fixed, antibody-labeled and FACS-purified MNs. (See also Figure S2, File S1)

(A) Schematic of the MN purification procedure by MARIS. MN cultures were digested into single cells, fixed and permeabilized before incubating with a specific HB9 antibody. HB9^{+} cells were sorted and collected. After reversal of crosslinks by proteinase K, RNA was isolated.

(B) A representative Bioanalyzer trace showing the 18S and 28S rRNA peaks from RNA isolated by MARIS. RNA integrity number (RIN) of more than 7.5 indicates intact RNA.

(C) Quantitative PCR analysis showing enrichment of MN markers in HB9^{+} sorted fraction compared to HB9^{-} cells. As a control, the HUES3 HB9:GFP reporter cell line was used and fold changes were normalized to HB9:GFP-negative cells.

(D) Transcriptome analysis revealed 911 differentially expressed genes (fold-change cut-off = 1.5; p-value < 0.01) in SMA MNs compared to wild-type MNs, with majority being upregulated in SMA MNs.

Author Manuscript Author Manuscript Author Manuscript Author Manuscript

(E) Selected enriched reactome gene sets elucidated by GSEA. Gene sets related to the ER stress pathway are highlighted.

(F) Table showing selected genes related to the ER stress pathway that are upregulated in SMA MNs. Their respective fold changes measured by RNA-seq are as shown.

Author Manuscript Author Manuscript Author Manuscript Author Manuscript

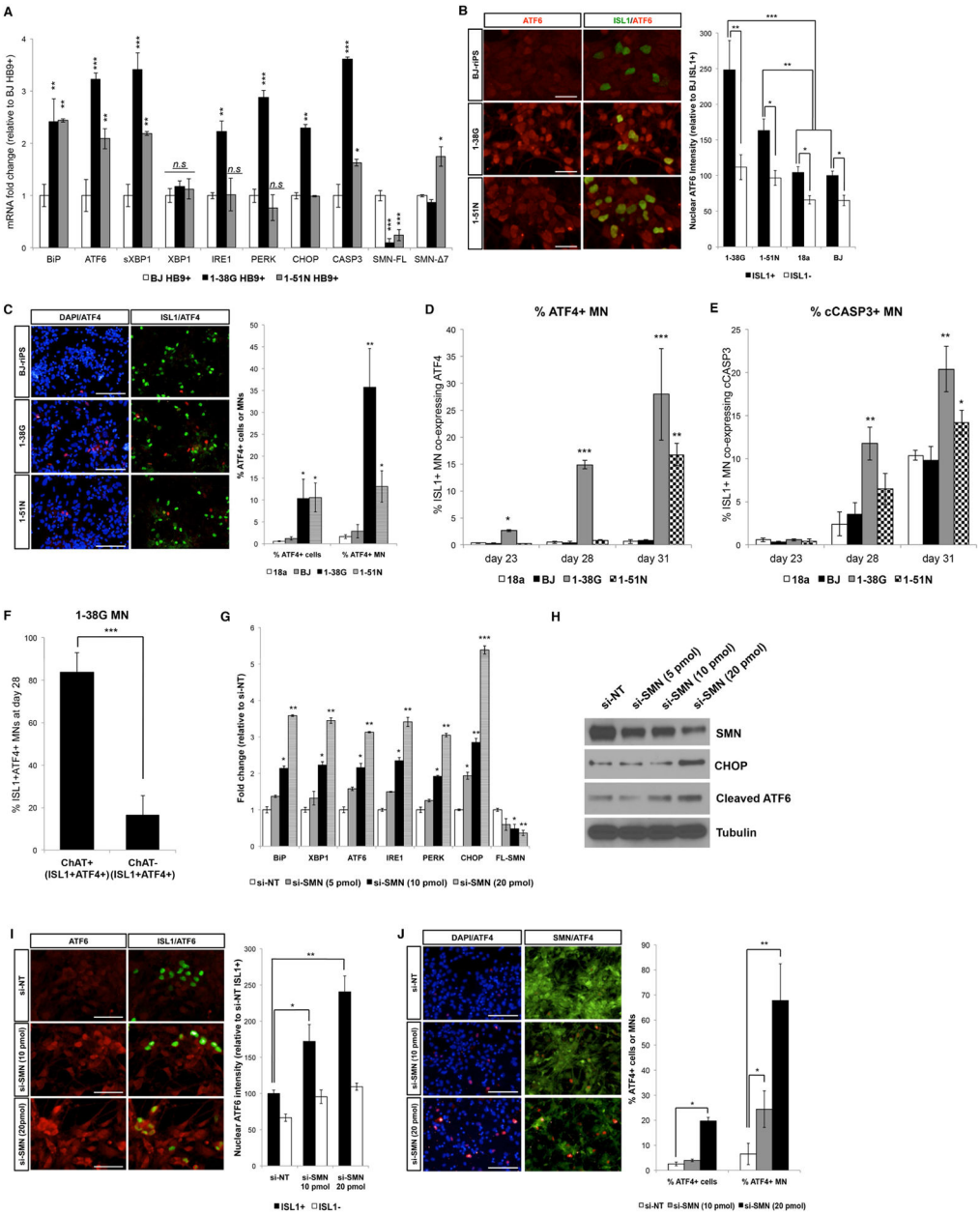

Figure 3. SMN-deficient cells express higher levels of ER stress markers (See also Figure S3 and Table S2)

(A) Quantitative PCR of FACS-purified HB9^{+} MNs derived from wild-type and SMA cultures at day 31. SMA MNs from 1-38G and 1-51N show higher expression of ER stress markers. Only 1-38G MNs show increased expression of markers characteristic of chronic ER stress: *PERK*, *CHOP* and *CASP3*. Gene expression is normalized to *GAPDH*.

(B) Co-staining of MN marker ISL1 (green) and ER stress marker ATF6 (red) in wild-type and SMA MN cultures. Scale bar indicates 25 μm. Nuclear ATF6 intensities of ISL1^{+} and ISL1^{-} cells are also measured.

Author Manuscript Author Manuscript Author Manuscript Author Manuscript

(C) Co-staining of motor neuron marker ISL1 (green) and ER stress marker ATF4 (red) in wild-type and SMA MN cultures. Scale bar indicates 100 μm. The graph depicts percentage of $ATF4^+$ cells in whole cultures, as well as percentage of $ISL1^+$ MNs co-expressing ATF4.

(D–E) Quantification of $ISL1^+$ MNs co-expressing ATF4 and cCASP3 respectively at days 23, 28 and 31, showing increasing ER stress over time, co-incident with increased apoptosis in SMA MNs.

(F) Immunostaining analysis indicating that majority of MNs undergoing ER stress ($ISL1^+$ $ATF4^+$ MNs) also co-express ChAT.

(G–H) qPCR and western blot analyses respectively show that knockdown of SMN in wild-type BJ-riPS MNs increased UPR target gene expression in a dose-dependent manner.

(I) Co-staining of ISL1 (green) and ATF6 (red) in wild-type MNs transfected with non-targeting siRNA (si-NT) and SMN siRNA (si-SMN) at the indicated dose. The scale bar indicates 50 μm. Increase in nuclear ATF6 intensity upon SMN knockdown is graphically represented.

(J) Co-staining of ISL1 (green) and ATF4 (red) in SMN knockdown BJ-riPS cultures. Scale bar indicates 100 μm. The graph shows increase in percentage of total cells and $ISL1^+$ MNs co-expressing ATF4 in SMN knockdown conditions.

Author Manuscript Author Manuscript Author Manuscript Author Manuscript

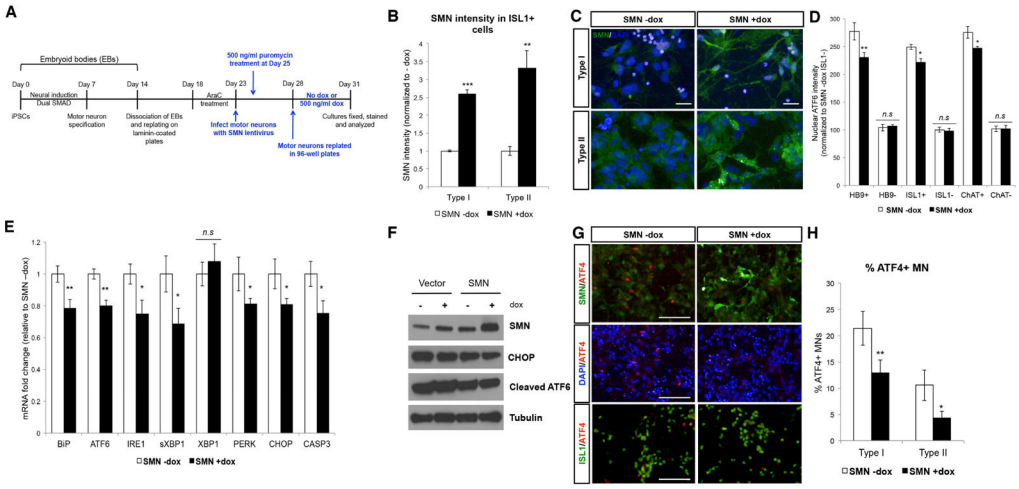

Figure 4. Increasing SMN expression reduces ER stress in SMA MNs. (See also Table S2)

(A) Experimental outline of lentiviral infection to achieve SMN overexpression in Types I and II SMA MN cultures.

(B) Quantitative measurement of SMN intensity indicates that SMN expression is 2.6-fold higher upon doxycycline addition in Type I MNs and 3.2-fold higher in Type II MNs.

(C) Immunostaining showing SMN overexpression (in green) after 3 days induction with 500 ng/ml doxycycline. Cellular nuclei are counterstained with DAPI. The scale bar indicates 50 μm.

(D) Quantitative assessment of nuclear ATF6 intensity in various MN populations ($HB9^+$, $ISL1^+$ and $ChAT^+$) with and without doxycycline induction SMN overexpression showing significant reduction of nuclear ATF6 levels in each of the MN populations, while the non-MNs ($HB9^-$, $ISL1^-$ and $ChAT^-$ populations) remain unchanged.

(E) Overexpression of SMN in Type I MN cultures reduces UPR target gene expression by qPCR.

(F) Western blot showing reduced ER stress markers upon SMN overexpression in Type II MNs.

(G) Co-staining of ISL1, SMN and ATF4 showing fewer $ATF4^+$ cells upon SMN overexpression in Type II MN cultures.

(H) Quantification of $ATF4^+$ MNs in Types I and II SMA MN cultures upon SMN overexpression.

Author Manuscript Author Manuscript Author Manuscript Author Manuscript

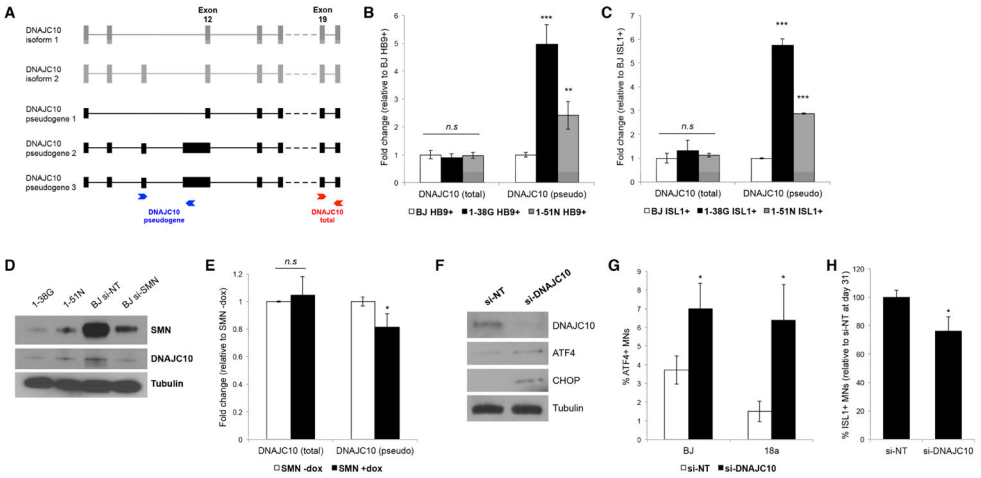

Figure 5. The ER chaperone *DNAJC10* is abnormally spliced in SMA MNs. (See also Figure S4)

(A) Schematic showing the 5 isoforms of *DNAJC10*, and primers used in this study to distinguish between *DNAJC10* pseudogenes (blue) and total *DNAJC10* transcripts that detects all 5 isoforms (red).

(B–C) qPCR measuring total *DNAJC10* transcript levels and *DNAJC10* pseudogene levels in HB9$^+$ purified MNs and ISL1$^+$ purified MNs respectively indicating that SMA MNs express more pseudogene transcripts even though total *DNAJC10* levels were unchanged. Notably, Type I MNs, which has least SMN, express the most *DNAJC10* pseudogene transcripts.

(D) Western blot showing that SMA MN cultures express less DNAJC10 protein compared to wild-type MNs. In addition, when SMN is depleted in wild-type MNs (BJ si-SMN), DNAJC10 protein levels also decreased.

(E) Overexpression of SMN in Type I SMA MNs reduces *DNAJC10* pseudogene expression without changing total *DNAJC10* levels.

(F) Depletion of DNAJC10 by siRNAs in wild-type MNs led to induction of chronic ER stress markers ATF4 and CHOP.

(G) Knockdown of DNAJC10 in two wild-type lines increased percentage of ISL1$^+$ MNs co-expressing ATF4.

(H) Depletion of DNAJC10 reduced number of ISL1$^+$ MNs.

Author Manuscript Author Manuscript Author Manuscript Author Manuscript

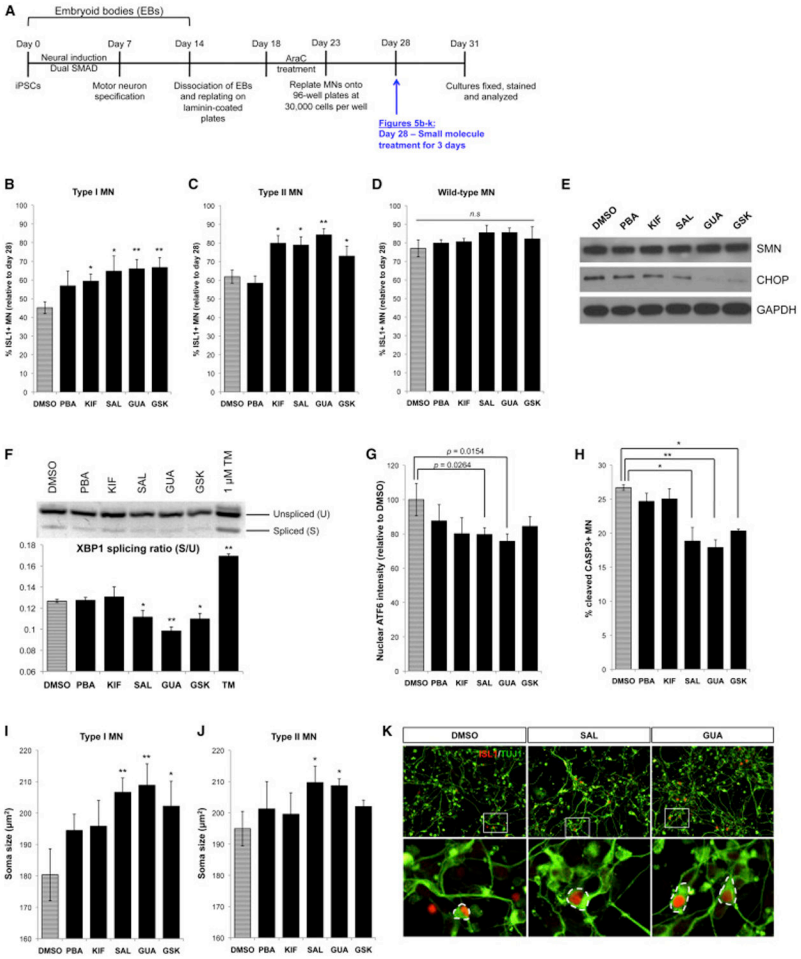

Figure 6. Small molecule inhibitors of ER stress rescue SMA MNs without increasing SMN protein levels. (See also Figures S5, S6 and Table S1)

(A) Experimental outline of ER stress inhibitor treatment on MN cultures. Cultures were treated for three days, starting from day 28, and analyzed at day 31.

(B–C) Percentage of ISL1^{+} MN after ER stress inhibitor treatment in SMA Type I (1-38G), and Type II (1-51N) cultures respectively. Values are normalized to number of MNs plated at day 28.

(D) Percentage of ISL1^{+} MNs after ER stress inhibitor treatment in wild-type (BJ) MN cultures. The values were not significant (*n.s*).

(E) Western blot of Type I MN cultures treated with the various ER stress inhibitors indicating that SMN levels remained the same while CHOP protein is reduced.

(F) Spliced XBP1 assay performed on SMA Type I MN cultures treated with DMSO, ER stress inhibitors and 1 μM tunicamycin (TM) as positive control.

(G) Measurement of nuclear ATF6 intensity in SMA Type I MN cultures treated with the indicated compound.

(H) Quantification of cleaved Caspase3^{+} MNs in SMA Type I MN cultures treated with the indicated compound.

(I–J) ER stress inhibitor treatment increases soma size of Type I and Type II SMA MNs respectively.

Author Manuscript Author Manuscript Author Manuscript Author Manuscript

(K) Representative images of Type I SMA MN cultures treated with DMSO, SAL or GUA, stained with ISL1 and TUJ1. Magnified images of the white boxes are shown in the bottom panel. The white-dotted circumference represents the measured soma sizes.

Author Manuscript Author Manuscript Author Manuscript Author Manuscript

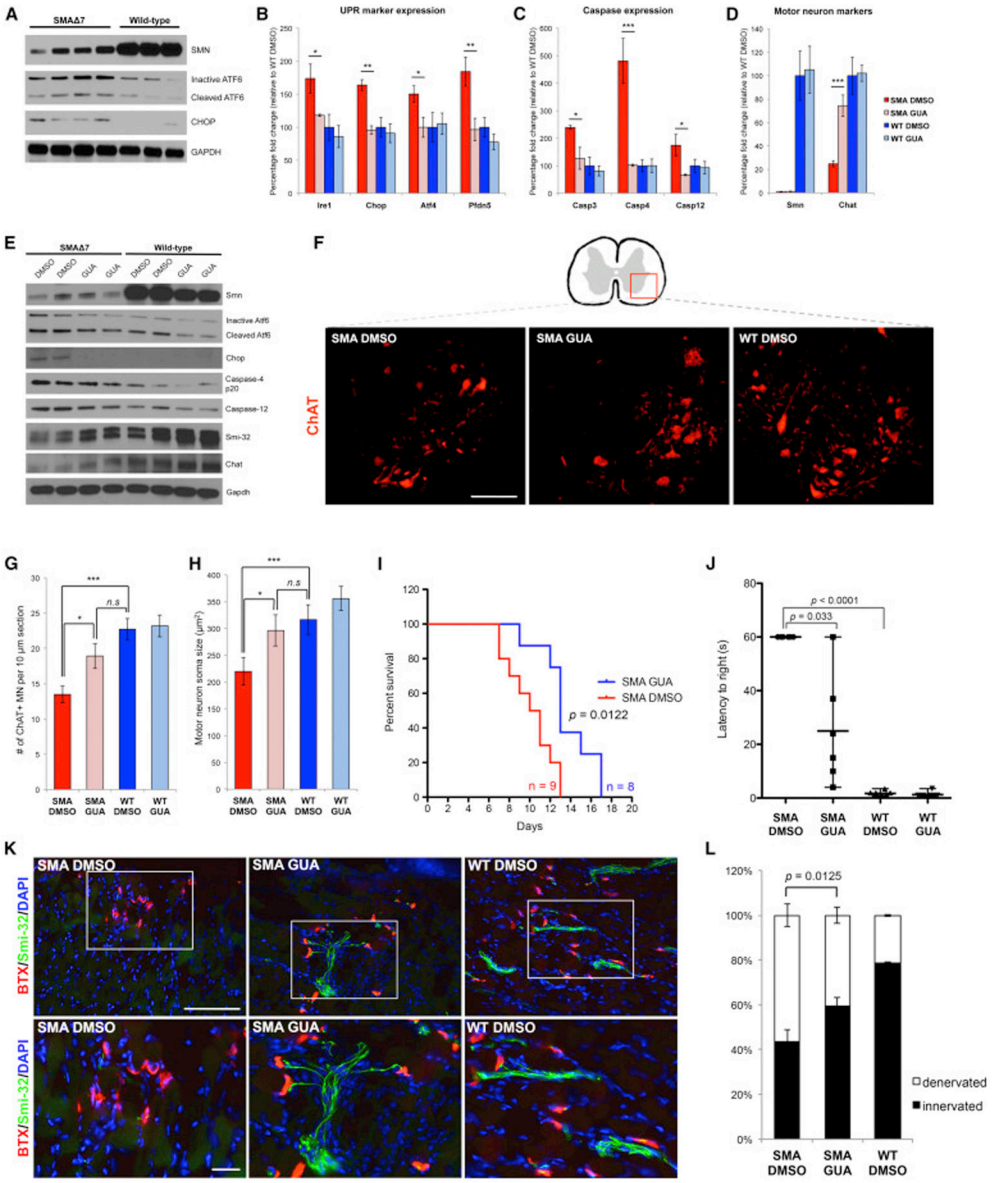

Figure 7. Guanabenz reduces UPR in spinal cords of SMA mice, and increases ventral horn MN survival. (See also Figure S4 and Table S3)

(A) Immunoblotting of spinal cord lysates from 4 SMAΔ7 mice and 3 wild-type mice at PND12. Spinal cords from SMAΔ7 mice show low expression of the full-length SMN protein, and higher levels of UPR markers cleaved Atf6 and Chop.

(B) GUA treatment results in reduction of *Ire1*, *Chop*, *Atf4* and *Pfdn5* mRNA expression in spinal cords of SMAΔ7 mice, to levels similar in control wild-type mice.

(C) Decreased *Caspase-3* expression, as well as ER stress-associated *Caspase-4* and *Caspase-12* expression was observed in spinal cord lysates of SMAΔ7 mice treated with GUA.

(D) While mRNA levels of *Smn* remain low in the SMAΔ7 animals, expression of the MN marker ChAT increases in the GUA-treated animals.

Author Manuscript Author Manuscript Author Manuscript Author Manuscript

(E) Western blot analysis of spinal cord lysates of SMAΔ7 and wild-type mice, treated with either DMSO or GUA, showing that GUA reduced UPR marker expression but led to increased MN markers Smi-32 and ChAT.

(F) Representative images of ventral horn $ChAT^+$ MNs (red) of the respectively treated animals. Scale bar represents 100 μm.

(G) Quantification of the number of $ChAT^+$ MNs in the ventral horns of each 10 μm section. 4–6 animals from each condition, and 20 lumbar sections representing the entire lumbar spinal cord were analyzed. Error bars are mean ± S.E.M.

(H) Measurement of soma sizes of $ChAT^+$ ventral horn MNs indicating that the average MN size of SMAΔ7 animals treated with GUA is significantly larger than DMSO-treated SMAΔ7 animals.

(I) Kaplan-Meier survival curve of SMAΔ7 mice treated with either DMSO (n = 9) or GUA (n = 8). Survival increased by approximately 35% (4 days) upon GUA treatment (p = 0.0122).

(J) Righting reflex time of DMSO and GUA-treated mutant and wild-type animals indicating that GUA-treated SMAΔ7 mice have significantly reduced righting reflex compared to DMSO controls (p = 0.033).

(K) Neuromuscular junctions (NMJs) of hindlimb muscles stained with α-bungarotoxin (BTX) and neurofilaments are identified by Smi-32 staining. Denervated NMJs are evident in DMSO-treated SMAΔ7 mice whereas the same region in GUA-treated SMAΔ7 animals showed preservation of NMJ innervation, similar to a wild-type animal. Magnified images of the white boxes are shown in the bottom panel. Scale bars represent 100 μm.

(L) Analysis of innervation status of hindlimb NMJs in respective treated mice. NMJs are scored as innervated when there is Smi-32 staining of neurofilaments at the NMJs. GUA treatment in SMA mice led to a 20% increase in innervated NMJs (p = 0.0125).